Rock Mechanics and Rock Engineering
https://doi.org/10.1007/s00603-018-1558-2

ORIGINAL PAPER

Extension Strain and Rock Strength Limits for Deep Tunnels, Cliffs, Mountain Walls and the Highest Mountains

Nick Barton[1] · **Baotang Shen**[2]

Received: 13 March 2018 / Accepted: 24 July 2018
© Springer-Verlag GmbH Austria, part of Springer Nature 2018

Abstract

Brittle rock can fail in tension even when all principal stresses are compressive. The culprit is Poisson's ratio, but marked stress anisotropy due to a neighbouring free surface, and due to a raised principal tangential stress is also necessary. Extension strain-induced failure causes fracture initiation in tension. Propagation in unstable shear may occur if the tunnels or mine openings are deep enough, and if they are located in hard, brittle, sparsely jointed rock. Both in laboratory uniaxial compression test samples with strength σ_c and in deep tunnels, extension fracturing and acoustic emission begin when the principal applied or induced stress reaches the magnitude of tensile strength divided by Poisson's ratio σ_t/ν. The traditionally expected fracture initiation when the principal or maximum tangential stress σ_1 or $\sigma_\theta = 0.4 \pm 0.1 \times \sigma_c$ can actually be explained with arithmetic. Using related logic, cliffs and the near-vertical mountain walls frequented by rock climbers, may have erosional or glacial origin, but extension strain limits their height, including vertical walls of sheeting joints and long continuous fractures. Shear failure seems to be reserved for occasional major rock avalanches. Equations with soil mechanics origin involving Coulomb parameters c and φ and density that may apply to vertical cuts in soil, give greatly exaggerated heights for rock cliffs and mountain walls since rock is brittle and favours failure in tension. Tensile strength, Poisson's ratio and density are suggested for estimating the maximum heights of rock cliffs and mountain walls, not compression strength and density. However, overall mountain heights are limited by critical state maximum shear strength, or by the slightly lower brittle–ductile transition strength.

Keywords Extension strain · Tensile strength · Poisson's ratio · Shear strength · Fracturing · Tunnels · Cliffs · Mountain walls · Mountains

Abbreviations

σ_c	Uniaxial compression strength (of rock)
q_c	Unconfined compression strength (of soil)
σ_t	Uniaxial tensile strength (of rock)
ν	Poisson's ratio
σ_h	Minor horizontal principal stress
σ_H	Major horizontal principal stress
σ_v	Vertical principal stress
σ_1	Major principal stress
σ_3	Minor principal stress
k_0	Ratio of σ_h/σ_v
K_0	Ratio of σ_H/σ_v
σ_θ	Maximum tangential stress (also σ_{max})
SRF	Stress reduction factor (from Q-value)
R_f	Depth of failure + excavation radius (a)
FRACOD	Fracture mechanics numerical code
DDM	Displacement discontinuity method
NGI	Norwegian Geotechnical Institute
Q	Rock mass quality
ε_3	Lateral extension strain (radial)
ε_t	Critical extensional strain
E	Young's modulus
$E' = E/(1-\nu^2)$	For plane strain
H_c	Critical height of vertical cutting in soil
C	Cohesion of soil (or intact rock)
φ	Friction angle of soil (or intact rock)
γ	Density of soil (or intact rock)
JRC	Joint roughness coefficient
JCS	Joint wall compression strength
R	Equivalent roughness of broken rock, screes
S	Equivalent strength of broken rock, screes

✉ Nick Barton
nickrbarton@hotmail.com

[1] NB&A, Fjordveien 65c, Høvik 1363, Norway

[2] CSIRO Energy, Kenmore, QLD, Australia

Published online: 21 August 2018

τ	Shear stress along potential rock-failure plane
T	Shear resistance, *N* normal resistance
σ_{xx}	And σ_{zz} horizontal and vertical stress components
φ_r	Residual friction angle of potential rock-failure plane
φ_b	Basic friction angle of flat rock surface
φ_c	Friction angle subtended by critical state ($\tan^{-1}$ ½)
σ_n	Normal stress acting across potential rock-failure plane
τ_{max}	Maximum (critical state) shear strength of intact rock
$\sigma_{3critical}$	Confining pressure needed to reach critical state τ_{max}

1 Introduction: Fracturing Modes in Tunnels

The first TBM tunnel in the world (credited to Beaumont 1880 but actually English 1880), failed along its haunches when it passed beneath a 70-m-high chalk cliff next to the future Channel Tunnel, which was built 110 years later. The massive fracturing is illustrated in Fig. 1. Clearly the mode of behaviour was very different to some sub-sea conditions experienced in an early part of the 1990s Channel Tunnel TBM excavations (Ch. 20–24 km), where three joint sets and smooth planar joints allowed over-break and an unexpected inflow of some sea water. Designers had not expected the weak chalk marl to be jointed. Barton and Warren (1995). The over-break delayed PC element ring building, and the dripping sea water, flowing through a rock mass with unexpected connectivity, damaged electrical equipment on the TBM.

The latter was joint-controlled behaviour, but that illustrated in Fig. 1 was some form of crushing of the $\sigma_c = 4$ to 9 MPa chalk marl. In the 1990s Channel Tunnel project, TBM world records were broken, such as best day, week and month of 75, 428 and 1719 m for 8 to 9 m diameter TBM. (Data from Robbins, reproduced in Barton 2013). The reason for these records, following the difficult conditions referred to earlier, was now a relative lack of jointing, and an ideal, low resistance to cutting, $\sigma_c = 4$ to 9 MPa rock (Table 1). So what was the mechanism causing the failure shown in Fig. 1 Was it failure in tension or failure in shear?

Joint industry (petroleum company) research that was conducted in NGI in the late 1980s, in contrast to the above mixed mode of fracturing, consistently demonstrated log-spiral shear failure phenomena, as seen in Fig. 2. This was probably due to the very high boundary stresses that were applied to the cubic samples, prior to drilling at different angles in relation to the usually unequal, flat-jack applied, principal stresses. (Addis et al. 1990). Shear displacement along the 'spirals' was verified with pre-drilled miniature boreholes back-filled with cemented coloured sand. (Bandis, pers. comm. 1986).

When a rock mass consisting of hard brittle rock is sparsely jointed, and at sufficient depth, simulations using FRACOD clearly show the propagation in shear that resembles log-spiral patterns. When different degrees of jointing are also present, there is a degree of dissipation of the need for fracturing, as shown in the four cases illustrated in Fig. 3. Details of these hard rock granite-simulating models can be found in Barton and Shen (2017).

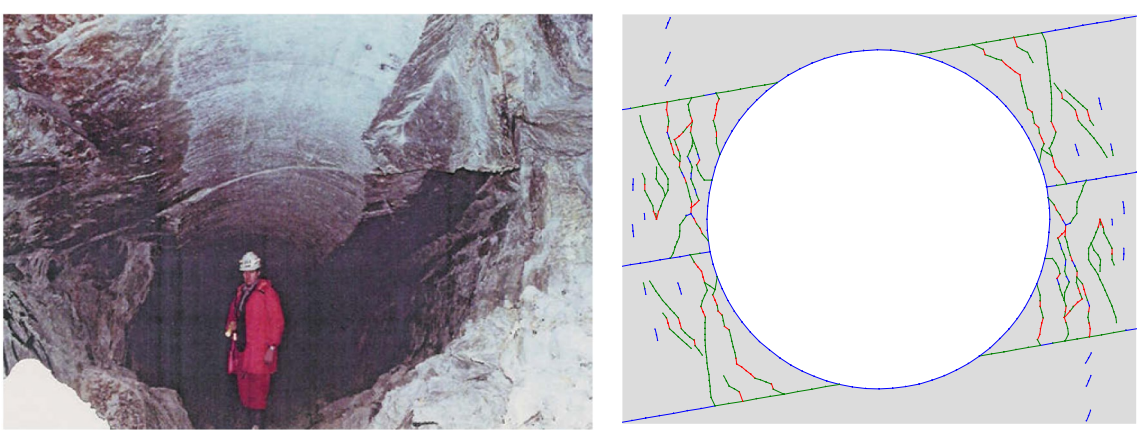

Fig. 1 The 2.2 m diameter Beaumont/English TBM tunnel from 1880, demonstrating assumed extension and shear failure when passing beneath a 70-m-high cliff close to the future 1990s UK–France Channel Tunnel. On the right is a fracture mechanics based FRACOD model (Shen et al. 2014). The most realistic model had assumed boundary stresses of $\sigma_h/\sigma_v = k_0 = 0.33$, which appears logical in view of the proximity of an adjacent cliff face and sloping shore line. The bedding planes are assumed, based on the single structure seen in the arch. (Note: red = tensile failure, green = shear failure)

Table 1 The input data that were assumed for the FRACOD model of chalk marl shown in Fig. 1

Property for FRACOD model	Value assumed
Young's modulus E	0.6 GPa
Poisson's ratio ν	0.25
Density	2000 kg/m^3
σ_c	6 MPa
Internal friction angle ϕ	30°
Cohesion c	1.73 MPa
Tensile strength σ_t	0.173 MPa
Fracture toughness K_{IC}	0.1 MPa m$^{1/2}$
Fracture toughness K_{IIC}	0.2 MPa m$^{1/2}$
Depth of cover	120 m
Vertical stress σ_v	2.4 MPa
$\sigma_H/\sigma_v = k_0$	0.33
Bedding plane dip, spacing	10°, 1 m
Bedding plane c and φ	0 MPa, and 20°

2 Two Common Empirical Rules in Tunnelling

In ultra-deep or highly stressed excavations in hard rock, both from the worlds of mining, nuclear waste underground research laboratory (URL) research, and from deep road tunnels, we have come to expect increased depth of break-out when the ratio of the maximum estimated tangential stress, and the uniaxial compression strength $\sigma_\theta/\sigma_c > 0.4$ (± 0.1). This follows from a Canadian initiative (Martin et al. 1998). The concept together with some data is shown in Fig. 4. Since an earlier date we have used a rapidly accelerating value of the stress reduction factor SRF in the single-shell Q-system tunnel support recommendations, when the same ratio σ_θ/σ_c exceeds 0.4–0.5, as shown in Table 2. Barton et al. (1974) also showed SRF deliberately accelerated when the simpler ratio of σ_c/σ_1 reduced to below 5. Why do we need to reach a peak tangential stress of only 0.3–0.5 $\times \sigma_c$ to reach fracture initiation? Is this due to a scale effect on σ_c, or is it due to an incomplete or incorrect assumption about rock fracturing behaviour?

Fig. 2 When principal stresses are even higher than σ_c as in these polyaxial drilling experiments to simulate deep well bores in sandstone, then fracture propagation by log-spiral shearing is the dominant failure mode. Addis et al. (1990). Log-spiral drawing from Bray (1967)

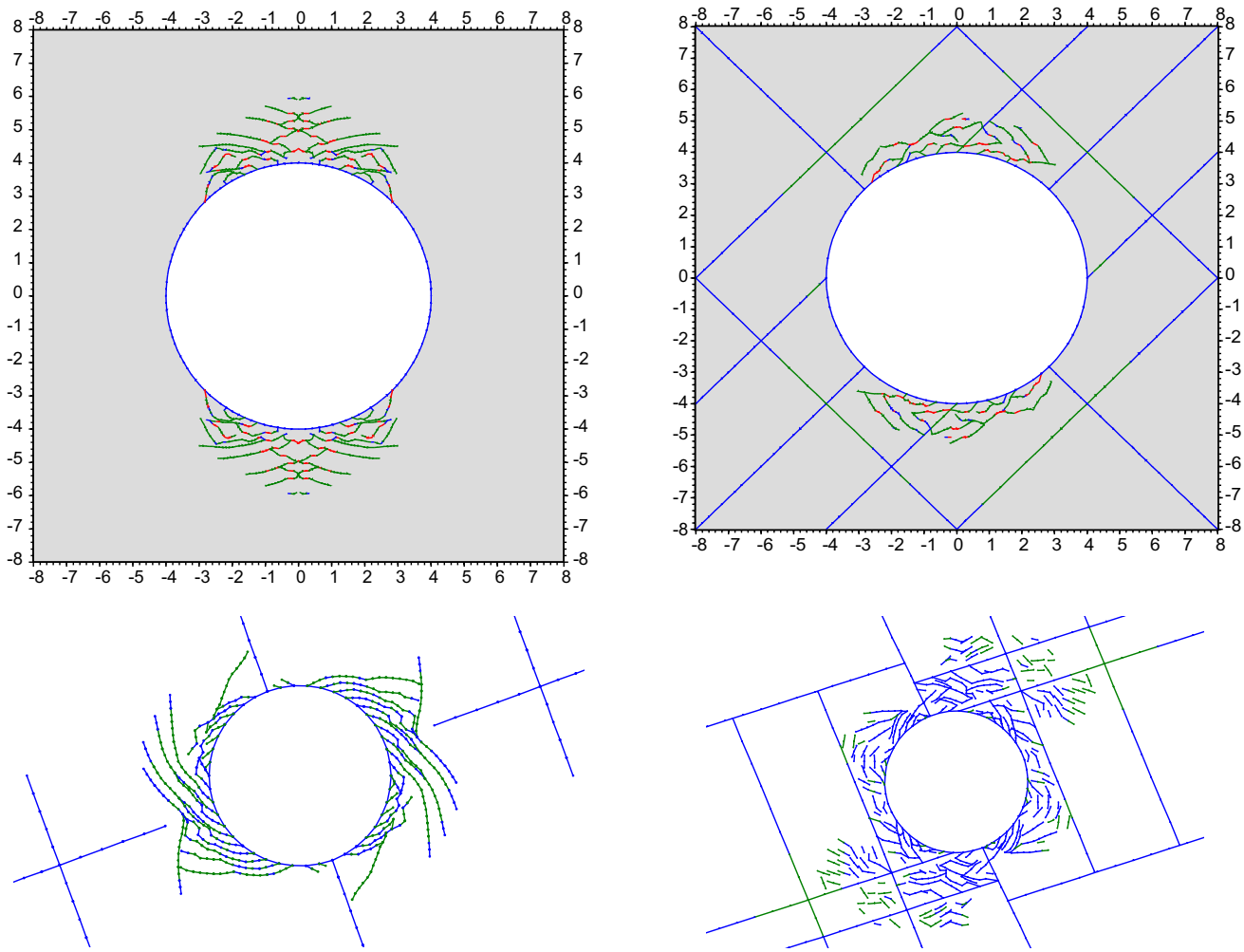

Fig. 3 Log-spiral shear fracturing tendencies when jointing is sparse and simulated stress levels are high enough. Top: 1000 m depth with $\sigma_h/\sigma_v = 2$. Bottom: major principal stresses of, respectively, 55 MPa (vertical) and 60 MPa (horizontal) in exploration of possible fracturing in a deep trans-Andean tunnel (Olmos) which suffered a lot of predicted rock bursting

The real answer to the '0.4 ± 0.1 question' is actually very simple, but was not discovered until recently, when the second author was developing a new sub-routine for the DDM-based fracture mechanics code FRACOD, which as we have seen, is capable of modelling discrete tensile (extension) fracture initiation and propagation in shear, both in intact and jointed models of deep tunnels in hard–brittle rock masses. Both mode I and mode II fracture toughness are utilized, and illustrated in Figs. 1 and 3.

3 Extension Strain-induced Tensile Fracturing

Based on extension strain theory, which was promoted by Stacey (1981), if the strain in a given direction becomes tensile and reaches a critical value, tensile fracturing will occur. A two-dimensional equation for expressing extension strain (in the lateral direction) is as follows:

$$\varepsilon_3 = \left[\sigma_3 - \nu\sigma_1\right]/E' \tag{1}$$

where ν is the Poisson's ratio of the intact rock and E' is the generalised term for Young's modulus (E) ($E' = E$ for the plane stress condition; $E' = E/(1-\nu^2)$ for plane strain, i.e. when no expansion is permitted in the third dimension, along the tunnel).

Extensional strain may develop in a stress field where all principal stresses are compressive, due to the effect of Poisson's ratio. This explains why tensile fracturing can occur in the roof/wall of an underground opening where no tensile stress is expected. The only requirement will be that $\nu\sigma_1 > \sigma_3$, i.e. the disparity between the major principal stress (σ_1) and the minor principal stress (σ_3) needs to be high enough.

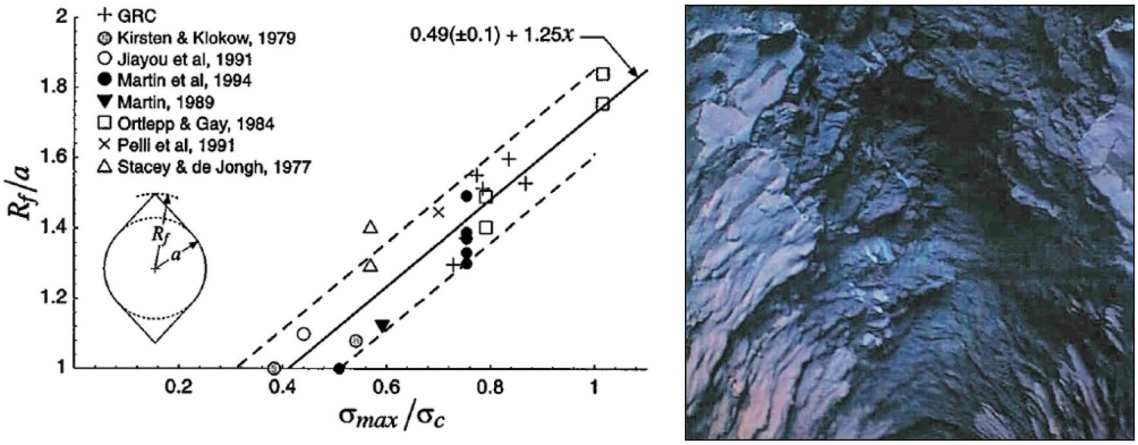

Fig. 4 Left: a method of interpreting (or predicting) depth of failure through 'over-stressing' (or over-straining, as about to be suggested) from Canadian and South African assemblies of data. Martin et al. (1998). In recent work Shen and Barton (2018) have indicated the limited area of tensile fracturing in the above figure, and where shearing is more likely to occur. Right: the photo is an example of one of five large river diversion tunnels from the Ita HEP in Brazil, where exceptionally high horizontal stress, even at less than 100 m depth, caused stress (i.e. strain-induced) fracturing in 200 MPa basalt. A K_0 ($= \sigma_H/\sigma_v$) principal stress ratio as high as 20 was back-calculated from $R_f = 10.5$ m, $a = 8$ m, ratio $\sigma_\theta/\sigma_c \approx 0.6$, $\sigma_\theta \approx 120$ MPa, because the vertical component of stress was as low as 2 MPa. Barton and Infanti (2004)

Table 2 The 'accelerating' value of SRF when the ratio $\sigma_\theta/\sigma_c \geq 0.4$, from the Grimstad and Barton (1993) analysis of 600 m to 1400 m deep road tunnels in Norway (Table 6b of Q-parameter ratings). Pre-1974 cases had suggested the following limits: $\sigma_c/\sigma_1 < 5$ or $\sigma_t/\sigma_1 < 0.33$ requiring higher SRF, and therefore, more robust shotcrete support, and reduced bolt spacing

(b)Competent rock, rock stress problems		σ_c/σ_1	σ_θ/σ_c	SRF
H	Low stress, near-surface, open joints	> 200	< 0.01	2.5
J	Medium stress, favourable stress condition	200–10	0.01–0.3	1
K	High stress, very tight structure. usually favourable to stability, may be unfavourable for wall stability	10–5	0.3–0.4	0.5–2
L	Moderate slabbing after > 1 h in massive rock	5–3	0.5–0.65	5–50
M	Slabbing and rock burst after a few minutes in massive rock	3–2	0.65–1	50–200
N	Heavy rock burst (strain burst) and immediate dynamic deformations in massive rock	< 2	> 1	200–400

The critical extensional strain (ε_t) for tensile fracturing can be determined using the tensile strength of the rock (σ_t). When a rock specimen is under unaxial tension ($\sigma_1 = 0$; $\sigma_3 = \sigma_t$), therefore:

$$\varepsilon_t = \sigma_t / E' \tag{2}$$

Using the critical extensional strain (ε_t) in Eq. (2) to replace ε_3 in Eq. (1) we obtain the critical compressive (i.e. tangential) stress for tensile fracturing (or spalling) to occur:

$$\sigma_1(\text{spalling}) = (\sigma_t + \sigma_3)/\nu \tag{3}$$

Considering that the confining stress σ_3 is zero at the wall of an underground opening, then for rocks with, typically $\sigma_c \approx 10\sigma_t$ and Poisson's ratio ≈ 0.25, tensile fracturing will start when the uniaxial (or tangential) stress reaches $\approx 0.4 \times \sigma_c$.

As suggested by the two empirical rules summarized earlier, many rock engineers, mining engineers and researchers have observed that tunnel spalling starts when the (isotropic, elastic) estimated maximum tangential stress (σ_θ) at the tunnel wall reaches approximately $0.4 \pm 0.1 \times \sigma_c$. (e.g. Martin et al. 1998), as shown in Fig. 4.

Similar spalling phenomena were experienced and recorded independently in deep Norwegian road tunnels. Barton and Grimstad (2014) reproduce the historic (pre-1990) case records from Grimstad, which show that the estimated ratios of σ_θ/σ_c were mostly in the range 0.4–0.8 for road tunnels of 600–1400 m depth where 'stress-slabbing' (extensional strain failure) and rock burst (shear failures) had occurred. These were the reason for strongly increased SRF in the Q-system tunnel support recommendations update of Grimstad and Barton (1993), for the case of massive rock (Table 2).

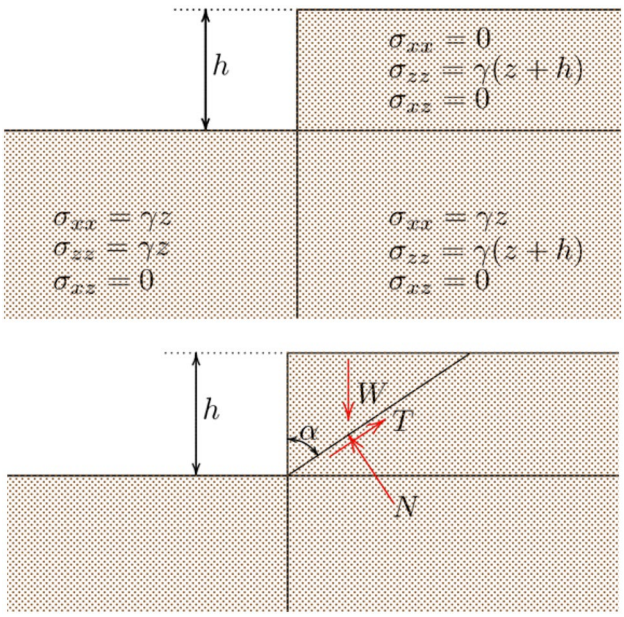

Fig. 5 Several approaches to the stability of a vertical cut appear in the soil mechanics literature. The top example (**a**) shows the assumed equilibrium of three zones and gives a lower bound solution. The bottom example (**b**) illustrates an upper bound solution involving a specific shear surface. Verruijt (2001)

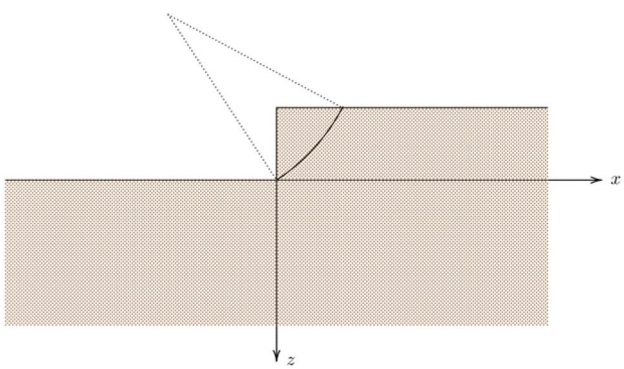

Fig. 6 The circular failure surface assumption used by Fellenius (1927)

4 Cliff Height Limit Formulations From Soil Mechanics

We will now take the question of rock fracturing 'outdoors', where there are added effects of temperature fluctuation, weathering, ice-wedging, etc. In a preliminary discussion of vertical cliffs, it will be convenient to refer to Figs. 5 and 6 which are borrowed from one of numerous recent soil mechanics texts, in this case following Verruijt (2001). First considering a purely cohesive material (with friction angle = 0°), and considering the equilibrium of the three distinct zones shown in Fig. 5a, it has been shown that the lower bound critical soil cutting (or cliff) height is:

$$H_c = 2c/\gamma \text{ (lowerbound, } \varphi = 0°) \tag{4}$$

It is (perhaps) known by those specializing in soil mechanics, that the 'exact' value of the multiplier (2) in Eq. 4 can be increased to 2.82, 3.39 and even to 3.64 by utilizing ever more realistic assumptions for the actually somewhat complex stress distributions in the three sectors illustrated in Fig. 5a (Verruijt 2001). The assumptions required for estimating the upper bound critical cliff height are illustrated in Fig. 5b. In this case a single plane shear surface is assumed. Expressing the weight of the wedge as ½ $h^2 \tan \alpha$, it can be shown that the upper bound critical cliff height, again for a purely cohesive material ($\varphi = 0°$) is given when $\alpha = 45°$. In this case:

$$H_c = 4c/\gamma \text{ (upperbound, } \varphi = 0°) \tag{5}$$

Using instead a circular slip surface (Fig. 6), Fellenius (1927) reportedly derived a lower value for the upper bound multiplier, of 3.83. So the highest lower bound and the lowest upper bound are seen to have the following narrow limits (Verruijt 2001).

$$3.64\ c/\gamma \leqslant H_c \leqslant 3.83\ c/\gamma \tag{6}$$

For the case of a linear Coulomb material with both cohesion and friction (c and φ), the lower bound and upper bound solutions just given must also include a friction angle, as in Eq. 7. Fellenius (1927) derived 3.85 for the multiplier, using a circular failure surface, while Drucker and Prager (1952) suggested using a log-spiral failure surface for greater realism. An exact solution is clearly elusive. However, in terms of the broad limits we can write:

$$2c/\gamma \tan(45° + \varphi/2) \leqslant H_c \leqslant 4c/\gamma \tan(45° + \varphi/2) \tag{7}$$

5 Preliminary Consideration of Cliffs Formed of Intact Rock

When considering rock and not soil, more complexity is involved in all of the above solutions because of various possible assumptions for stress distribution, and also because of strain and dilation-dependent material behaviour. For the case of (almost) intact rock, the medium of most interest to us from now on, we need to consider the strong non-linearity of the shear strength in the case of high mountain walls.

Since the nomenclature cliffs needs to be 'stretched' to mountain wall heights of 1 km or more, it is important to accept that both c and φ in Eq. (7) need to become stress-dependent variables. Figure 7 illustrates a promising scheme

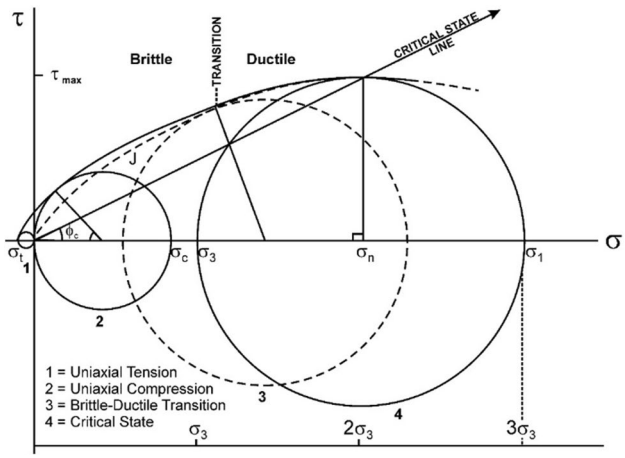

Fig. 7 The strongly non-linear shear strength of intact rock and the critical state concept defining maximum possible shear strength, from Barton (1976, 2013). (*Linear* Mohr–Coulomb does not apply over very large stress ranges). Note that Singh et al. (2011) confirmed that the values of σ_c and $\sigma_{3\ \mathrm{critical}}$ are equal or nearly equal for the majority of rock types. We therefore have the significant situation that $\tau_{max} \approx \sigma_c$ (numerically speaking). This has repercussions for the unexpectedly simple equation suggested by Terzaghi (1962), which can be shown not working for cliffs or steep mountain faces, but unexpectedly 'working' for the maximum heights of the world's highest mountains. (Fourteen are between 8 and 9 km in height). The probable importance of the critical state for these maximum heights is discussed later. Clearly the uniaxial (unconfined) compression strength as used by Terzaghi for steep mountain walls cannot be used under 8–10 km of rock cover

for the actual non-linearity, which was suggested a long time ago in Barton (1976), following a wide review of high-pressure triaxial tests on numerous rock types, mostly performed in the classic studies of Mogi (1966a, b) and Byerlee (1967, 1968). The critical state suggestion and the deviation from linear Mohr–Coulomb was quantified by Singh et al. (2011). More recently simple equations describing the continuously curved strength envelope have been developed by Shen et al. (2018). Curvature is greater than Hoek–Brown, as also shown by Singh et al. (2011).

With reference to the figure caption for Fig. 7, we now have to address the controversial Terzaghi (1962) suggestion of a classically simple but rather erroneous equation for the vertical height of rock cliffs. Various authors have emphasized that his equation greatly exaggerates (by a factor of three to four) the heights of known mountain walls. In fact, Terzaghi himself immediately (in the same paper) suggested the need for jointing to explain the much lower mountain wall heights seen in practice.

$$H_c = q_c/\gamma \text{ (soil terminology). Used by Terzaghi (1962)} \tag{8}$$

$$H_c = \sigma_c/\gamma \text{ (rock terminology). Used in this paper} \tag{9}$$

Let us now consider the example of a moderately strong rock with $\sigma_c = 50$ MPa. Terzaghi's Eq. (8) or (9) predicts a maximum cliff height of 2000 m, if rock density was just 2500 kg/m^3, such as for a typical sandstone. Granite with even a moderately reduced-by-weathering in situ σ_c of 100–150 MPa would suggest maximum vertical 'cliff heights' of 3600–4800 m if a density of 2750 kg/m^3 was assumed. Consistent units for this equation are kN/m^2, e.g. 100 MPa × 1000 to convert to kN/m^2, and density in units of kN/m^3 (e.g. 27kN/m^3 for granite), with acceleration due to gravity 9.86 m/s^2 already accounted for.

We know that such heights as 2.0, 3.6 and 4.8 km are impossible for vertical or near-vertical mountain walls, even in massive hard rocks such as granites, limestones, and sandstones. In the next section we will show some of the world's highest known mountain walls: which for instance have heights of approximately 750 m for sandstone, and approximately 1250 m for granite. The record may be 1340 m for the Great Trango Tower in the Karakoram mountain range in Pakistan. An error of 3:1 or even up to 6:1 is apparent, if trying to apply 'soil mechanics' solutions to a medium that is brittle, and therefore, usually fails in a different manner to soil.

However, when Terzaghi's Eq. (8) or (9) is applied to the maximum possible height of mountains, it may be 1:1 in apparent 'accuracy', but it is not consistent with the critical state logic shown in Fig. 7. His equation gives a reasonable looking result for the wrong reasons. Isostatic uplift ('floating' mountain chains), and the weakening effects of heating and pore pressure are all big uncertainties of where the estimation of equilibrium should be made: a sub-mountain depth of 10 km as a round figure might be a good starting point. With an assumed composite density of 2850 kg/m^3 and 8500 m of pore water pressure (both chosen for simplicity), a maximum rock 'compressive' strength of 200 MPa seems to be needed. In fact, the maximum possible shear strength of 200 MPa is the weakest link, compared to $\sigma_{1max} \approx 3\ \sigma_{3critical} \approx 3 \times \sigma_c = 600$ MPa. The 'logical' use of a confined compression strength for the highly confined situation at 10 km depth is clearly much too conservative.

Concerning the continued trial evaluation of 'soil mechanics' formulations summarized in Eq. (7), we need to make appropriate estimates of cohesion. The same 'sandstone' and 'granite' examples can be used again. Referring to Fig. 7 for convenience, a lower bound estimate of cohesion (c) would be obtained most simply by assuming a straight line, rather than the curved tangent between the uniaxial tension (σ_t) and uniaxial compression (σ_c) Mohr circles. The simple equation for this lower bound (c), derived from Mohr circle geometry, was given in Barton (1976):

$$c = {}^1\!/_2\,(\sigma_c.\sigma_t)^{1/2} \tag{10}$$

We can examine the above formulations with the same examples of a moderately strong valley wall sandstone ($\sigma_c = 50$ MPa) and a high mountain wall in granite (conservative $\sigma_c = 100$ MPa). Assuming that $\sigma_c/\sigma_t \approx 10$ (the range might be 5–20):

- Sandstone $\sigma_c = 50\,\text{MPa},\ \sigma_t = 5\,\text{MPa}$ $\quad c = {}^1\!/_2(50 \times 5)^{1/2} = 7.9\,\text{MPa}$
- Granite $\sigma_c = 100\,\text{MPa},\ \sigma_t = 10\,\text{MPa}$ $\quad c = {}^1\!/_2(100 \times 10)^{1/2} = 15.8\,\text{MPa}$

The gradient of the presently assumed straight line between the tensile and compressive strength Mohr circles, giving a lower bound value of c is given by:

$$\sigma_c/\sigma_t = \tan^2(45^\circ + \varphi/2) \tag{11}$$

A common friction angle φ of approximately 56° is indicated if $\sigma_c/\sigma_t = 10$. Using just the lower bound solution given by Eq. (7): $H_c = 2c/\gamma \tan(45^\circ + \varphi/2)$, serious errors are evident:

Sandstone cliff $H_c = 2 \times 7.9 \times 1000/25 \times \tan(45^\circ + 28^\circ) = 2067$ m

Granite mountain wall $H_c = 2 \times 15.8 \times 1000/27.5 \times \tan(45^\circ + 28^\circ) = 3759$ m

Using the 'soil mechanics' upper bound, i.e. the right-hand side of Eq. (7), these roughly 3:1 errors are doubled.

Except for the case of huge rock avalanches (Fig. 8c) seldom experienced in recorded history, it is clear that even this lower bound solution, borrowed from soil mechanics and based on shear strength, cannot be applied to vertical rock cliffs. So we remain in urgent need of a 'cliff formula' for brittle rock. Our solution is to combine Poisson's ratio (ν) and tensile strength (σ_t), from the 'tunnel-failure logic' of Eq. (3), with the assumed maximum vertical stress (γH/100) in MPa near the cliff face.

6 A New Formula for Vertical Cliffs and Steep Mountain Walls

Due to their pioneering drive and remarkable skills, mountain wall and Alpine-style rock climbers have been conquering the highest and steepest mountains and mountain walls for the last 60 years. Many first-ascent records of the highest mountains occurred in the 1950s, more competitive and free-solo mountain-wall climbing in the last 20 years has meant that the internet is generously supplied with hundreds of thousands of photographs. As 'desk-bound' researchers in relation to these daring climbers (and climbing photographers), the liberty has been taken to re-size a very few of the most illustrative cases, to aid in our exploration of rock fracturing processes caused by extensional strain, by exceedance of tensile strength, and by propagation in shear. One of the climbers illustrated later, considered this to be 'awesome' which we take as implicit approval of our objective.

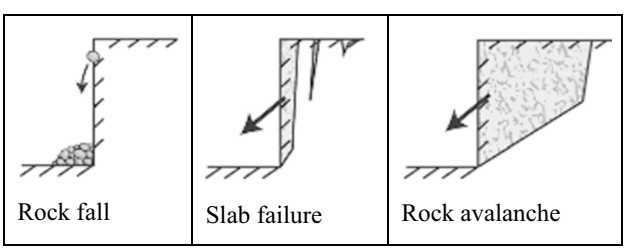

Fig. 8 Three of the principal cliff (or mountain wall) degradation and failure processes, as envisaged by Melosh (2011). These have been presented in this figure in the order of frequency-of-occurrence, using just three of Melosh's five categories

In popular rock-climbing meccas, like the Yosemite National Park in eastern California ('the valley' to American rock climbers), detailed records of the thousands of rock falls and occasional slab failures have been kept by the Park service, assisted by the USGS and others. Stock et al. (2012) contains a remarkable documentation of the first two categories shown in Fig. 8, from Melosh (2011). Fortunately the third category, the rock avalanche is a seldom, though devastating occurrence, with velocities and travel distances that defy understanding, unless one invokes instantaneous steam formation due to the heat-generated transformation of ground water to load-bearing steam. A case known to the writers (Marte Gutierrez, priv. comm.) saw rescue workers unable at first to dig down to a buried town many kilometers distant from the failed mountain side in the Phillipines. This was reportedly due to the high initial temperature of the rock and mud debris, which had even 'jumped' the far side of an intervening hill, leaving palm trees intact.

Before reproducing photographs of mountain walls, it may be helpful to visualize vertical stress distributions, using finite element analyses of a theoretical (less common) vertical cliff, and of a more typical, almost vertical situation. Figure 9 shows two such cases, from the cliff studies of Wolters and Müller (2008). The curved wall case corresponds well to the extreme mountain walls to be illustrated. Note the different sizes of the theoretical (isotropic, elastic, continuum) tension zones at the top of the modelled 'cliffs'. These zones are obvious areas for the initiation of degradation by tension crack formation, aided by water pressure, ice-wedging, internal block-wedging, and the constantly

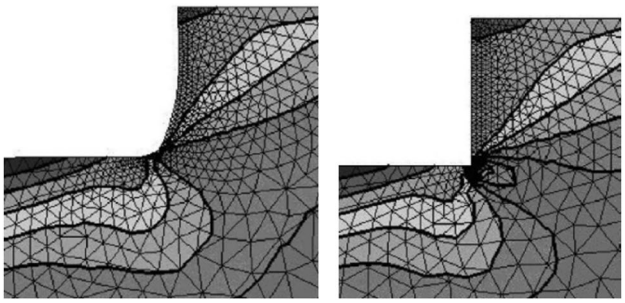

Fig. 9 FEM models of principal (vertical) stress for vertical and semi-vertical cliffs given by Wolters and Müller (2008). Their studies also showed that if a tension crack is modelled, 'a line' of high shear stress will tend to develop from the base of the crack to the highly stressed (and strained) toe of the slope

fluctuating temperature which is known to weaken all rocks. An excellent recent article on the subject from the Matterhorn, was published by Weber et al. (2016).

Four of the highest almost vertical mountain walls known to the world's climbing profession will be illustrated in Fig. 11. They are awe-inspiring to both layman and expert climber. They provide an interesting contrast to mountains which appear to show (prior) shear failure, or the effect of major joint sets (refer to Fig. 10), where high shear stresses in the past may have allowed such failure surfaces to develop in preference to the slab failures that can be assumed to have dominated in the gradual mountain degradation that we see in the high walls formed by the strongest brittle rocks.

Figure 11 shows some compelling evidence for the range of 'cliff' heights apparently made possible by the wide range of compression strengths of rock. The world's highest almost vertical mountain walls top out on either side of 1300 m. The probable record is 1340 m for the Great Trango Tower in the Karakoram, Pakistan. We may perhaps expect (laboratory-scale) compressive strengths of 100–150 MPa for the granites in these highest walls, while in the case of Cappadocia's ancient cliff dwellings in porous tuff in Turkey, the compressive strength may be only 1–2 MPa, limiting cliff heights to only 15–20 m. The key to the huge range of heights illustrated in Fig. 11 is that the tensile strengths of rocks may range from no more than 5–10 MPa for exposed granite, down to 0.05–0.1 MPa for exposed tuff. Numerous examples of the latter are given by Aydan and Ulusay (2003) from Cappadocia.

The foregoing review of classical soil-based equations has revealed (confirmed) their inadequacy when applied to failure of intact rock. The reasons can be easily explained. A trench failure or a cut-slope failure in soil, due to inadequate sheet-piling or inadequate soil-nailing, might involve 5, 10 or at most 15 m of failed excavation in the soil. For intact rock to fail in the (shear failure) manner of soils (Eq. 7), huge cohesive strength has to be overcome, perhaps as much as 5000–25000 kPa (5–25 MPa). One is immediately at mountain-scale for the necessary tens of MPa shear stresses to be generated. Alternatively, as immediately concluded by Terzaghi (1962), the rock has actually to be a jointed rock mass with sufficient planes of weakness. This is not disputed, but here we are examining how to explain the failure (or critical slope height) of mostly massive, sparsely or unjointed (and near-vertical) rock walls, such as illustrated in most of the cases shown in Fig. 11.

Due to the short-comings of soil failure theories for the case of (almost) intact rock, an alternative equation is suggested, based simply on equating the critical tangential (or principal) stress that will cause extensional failure (even in a compressive stress field) with the assumed vertical stress generated by the density and the height of the cliff or mountain wall under investigation.

Fig. 10 Presumed historic (conjugate) shear failures, or the influence of prior geologic structure. Photos selected from the Karakoram, Pakistan. Prior anisotropic stress is suggested, from different points up the curved failure envelope depicted in Fig. 7. Mohr circle logic suggests higher stress/strength ratios for the second case depicted, with its larger included angle

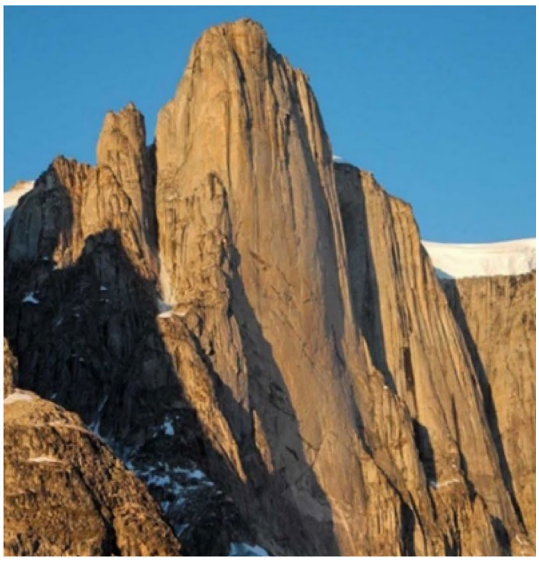

◂**Fig. 11** The top four photographs are examples of extreme mountain walls in hard or very hard rock. The bottom two are examples of cliffs in weaker and porous rock. From top, left-to-right: **a** Great Trango Tower, Karakoram, Pakistan: 1340 m, **b** Mirror Wall, Baffin Island, Canada: 1200 m, **c** El Capitan granites, Yosemite: 950–1000 m, **d** West Temple sandstones, Zion, Utah: 650–700 m, **e** Beachy Head bedded chalk, England: 75–100 m, **f** Cappadocia tuff, Turkey: 15–20 m

Tensile strengths presumably tend to get downgraded by weathering during millennia of thermal cycles, which may exceed a 70–80 °C annual range, and also vary strongly even during one day. The big range of what are in fact 'limited' cliff and mountain wall heights, can be roughly explained by comparing the assumed maximum vertical stress (the critical spalling stress in this case) with extensional strength σ_t/ν. To do this involves simply comparing cliff height and rock density, with the ratio of tensile strength and Poisson's ratio.

$$H_{\text{critical}} = 100\sigma_t/\gamma\nu \tag{12}$$

(where σ_t is tensile strength: MPa, γ is density: tons/m^3, and ν is Poisson's ratio). Note that the multiplier of 100 is purely a function of convenience when using typical rock mechanics strength units, expressed in MPa. With strength in kN/m^2 and density in kN/m^3 the '100' can be dispensed with.

Equation (12) has been tested with the examples reproduced in Table 3. To the extent possible using engineering judgement, realistic input values are employed, for a wide spectrum of possible rock conditions, ranging from uniaxial compression strengths of 150 MPa typical for hard granite, down to just 1.0 MPa which might be typical for a weakened porous tuff, as found in the historic cliff dwellings of Cappadocia, depicted at the bottom of Fig. 11.

In general, the ratios of compressive and tensile strengths for rock are in the range of $5 < \sigma_c/\sigma_t < 20$. In Table 3, since (compared to tunnels), cliffs and mountains are exposed to weathering and temperature fluctuation forever (or at least until the next glacial period), we have deliberately made relatively conservative estimates of tensile strength σ_t.

The proposed $\sigma_t/\gamma\nu$ mechanism of extension failure has the effect of steepening (or maintaining the prior steepness) of mountain walls and cliffs. The reason for the mountain faces to be so steep and high as at present presumably must be associated with their prior tectonic uplift followed by glacial sculpting. This would include that resulting from within the classic 'cirque' headwall structures seen in high mountain areas, if the responsible glacier has retreated enough for the near-vertical headwall to be exposed, and therefore, become unsupported.

The sketches and photographs presented in Fig. 12 show several aspects of the extensional mechanism. Because tensile strength is slowly reduced nearest to an exposed cliff or mountain face by constant cycling of temperature and moisture, it becomes easier for slabbing to occur. With assumed microcracking and grain-scale ice pressures, one may surmise an effective increase in Poisson's ratio, together with reduced near-surface tensile strength. If broadly correct, extension failure due to the σ_t/ν mechanism would become easier with time. This is probably the true cause of the relative frequency of slabbing due to the 'constant' propagation of sheet jointing. We will return to this subject later.

The estimation of basal shear strength could be based on a combination of the strength components JRC and JCS shown in Fig. 13, since a final 'cascading' of failure may be involved, for example: failure of remaining intact 'bridges', then shearing (or not) on these new, fresh, rough surfaces, then mobilization (or not) along the already established shear plane (prior tectonic structure) or suitably oriented major joints.

7 Sheeting Joints, 'Slabbing', Mountain Degradation

The limiting value of strength for determining cliff heights is the in situ scale effect on the tensile strength, already the minimum strength component, but undoubtedly reduced slowly with time, until a slabbing fracture can form. There was a recent slab failure in Yosemite Valley weighing several thousand tons, measuring approx. 30 × 60 × 0.65 m. When such a slab weakens and loosens, it accentuates the effect of temperature and moisture (and ice-wedging cycles) for the next layer of rock.

Dramatic photographs of rock climbing indicate that slab failures are what give the mountain face its (local) smoothness and planarity. Furthermore, the essential vertical crack paths loved (and needed) by climbers, that can run for hundreds of meters up some classic climbing routes, are very likely to be an expression of the same extensional strain mechanism acting in the third (along the wall) direction. Thermal stress due to temperature change adds to the high stress, and therefore, elevates the extensional strain, also causing increased slabbing. A huge industry of nuts and bolts and exotic expanders are designed to allow rock climbers to progress up vertical cracks of varying width. Concerning using these cracks, the record for 'The Nose' route up the 1000 m of El Capitan in the Yosemite Park was, until late in 2017, 2 h and 23 min. Hans Florin, who has more than 160 ascents up The Nose was partnered by arguably the world's foremost free-soloist, Alex Honnold. The first ascent, decades before, took 45 days, spread over 18 months of route preparation. Honnold is pictured in Figs. 14 and 18.

Although the rock surface curvature obviously helps for generating tensile stress as suggested by Martel (2017), it is not a necessary condition for generating sheeting joints. The classic curved sheeting joints on 'the back' of Yosemite's

Table 3 Examples of potential vertical height limits for near-vertical mountain walls and cliffs, over two orders of magnitude of assumed rock strengths, based on the application of Eq. (12)

$\sigma_c = 150$ MPa Very hard	$\sigma_c = 50$ MPa Medium hard	$\sigma_c = 15$ MPa Low strength	$\sigma_c = 1.0$ MPa Very low strength
$\sigma_t \approx 9$ MPa	$\sigma_t \approx 3$ MPa	$\sigma_t \approx 1$ MPa	$\sigma_t \approx 0.05$ MPa
$\nu = 0.25$	$\nu = 0.20$	$\nu = 0.15$	$\nu = 0.15$
$\sigma_t/\nu = 36$ MPa	$\sigma_t/\nu = 15$ MPa	$\sigma_t/\nu = 6.7$ MPa	$\sigma_t/\nu = 0.33$ MPa
$\gamma = 2.8$ ton/m^3	$\gamma = 2.5$ ton/m^3	$\gamma = 2.25$ton/m^3	$\gamma = 2.0$ ton/m^3
$H_{crit} = 1290$ m	$H_{crit} = 600$ m	$H_{crit} = 296$ m	$H_{crit} = 16$ m

Half Dome have alternative means of development than the curvature. The 750 m vertical front face is remarkably planar by comparison, and may have extension origin (Fig. 15). Sheeting joints are often planar over long distances, both horizontally and vertically, as can be vouched for by rock climbers, and as can be seen in tens of thousands of rock-climbing photographs. Interesting sources here are the following: Hall and Child (2002), Davis (2013), Honnold and Roberts (2016), Florine and Moye (2016).

Nevertheless, around the toe of steep high slopes in rock there are likely to be curved iso-lines of extension strain, as shown by Stacey et al. (2003), both from continuum modelling and conceptually. Curved extension fractures have also been modelled by FRACOD in this critical location as shown by Barton and Shen (2017). The base of El Capitan also shows such features in places, but screes presumably cover most of these.

For the case of the Cappadocia tuffs, careful studies by Aydan and Ulusay (2003) and others, have shown that temperature (freeze–thaw) cycling and moisture content cycling have a degrading effect on both compression and tensile strength. There may be an effective annual temperature range of 70–80 °C, even in the shade, and this may be increased for cliffs in direct sunlight, for some of each day, and for

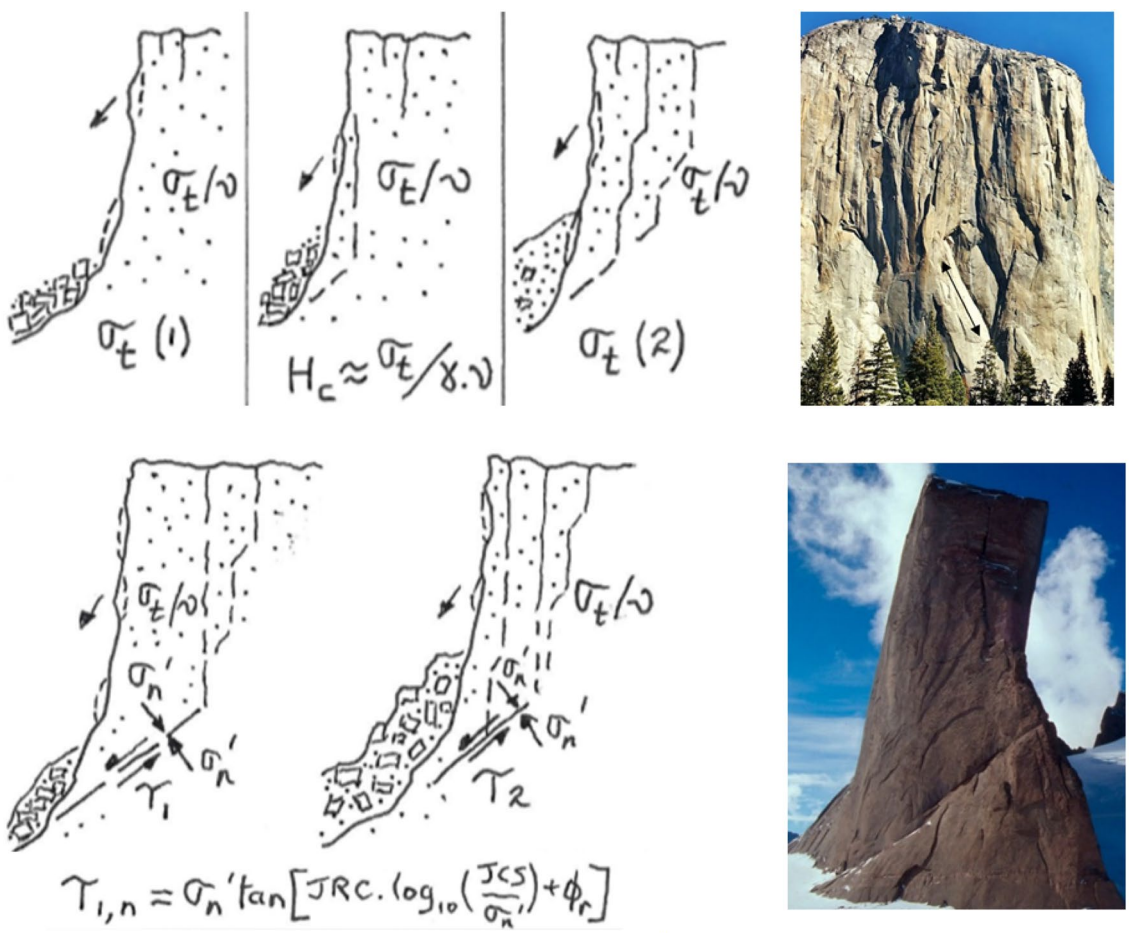

Fig. 12 Left: sketches illustrating the extensional strain failure mechanism involving the overcoming of the extensional strength σ_t/ν. Also shown is the possibility of rock avalanche-scale basal shear failures, due to adverse tectonic structures. The shear strength available along the basal discontinuities is likely to degrade with time, and 'intact bridge' shear-through will eventually represent a serious threat. The possibility of basal shear appears to be slightly developed at El Capitan in Yosemite, 1,000 m in height (top-right), but apparently well developed at Holtanna, a 750-m-high monolith, in Dronning Maud's Land, Antarctica (bottom-right)

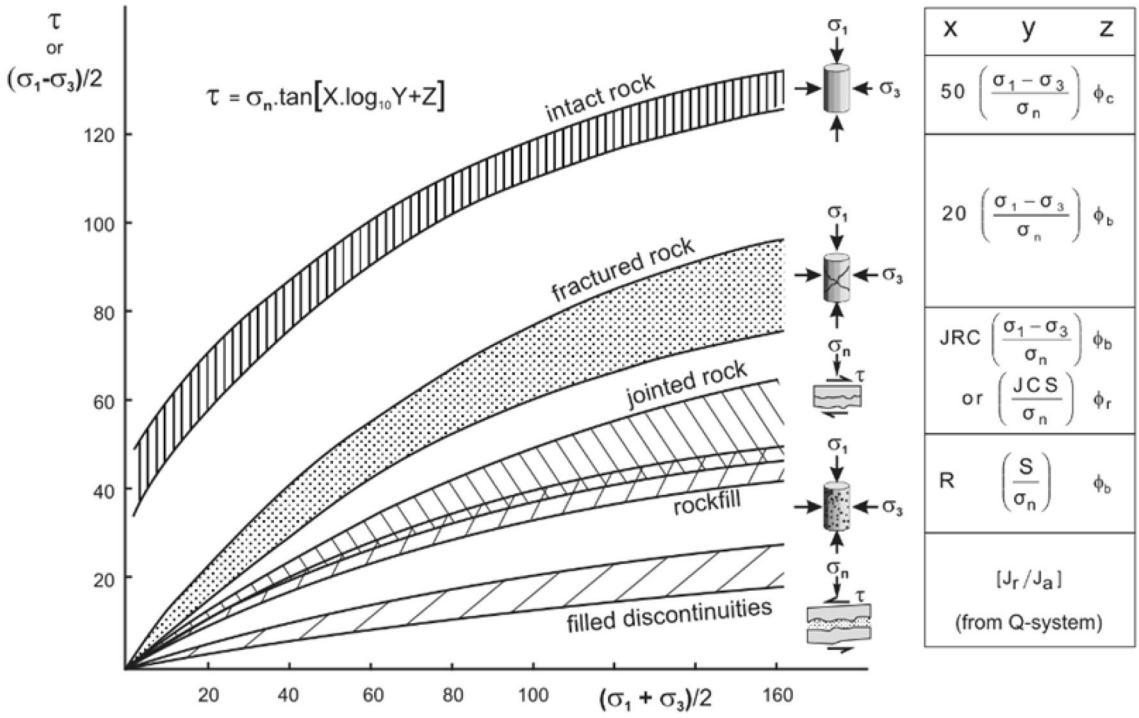

Fig. 13 Representation of shear strength components in the form of laboratory tests, from Barton (1999). Several components of strength may be involved when a large-scale body of rock is approaching failure. A cascade of shear resistance and its possible progressive defeat involves a shear strain- and displacement-dependent process, not a simple instantaneous Coulomb relation $\tau = c + \sigma_n \tan \varphi$, nor a Byerlee 'law' friction coefficient $\mu = 0.85$. These linear approximations are often misleading when a significant range of stress is involved, as emphasized by Barton (1976, 2013)

Free-solo ace, Alex Honnold on front face of Half Dome, Yosemite where he made the first ever free-solo ascent. Note active exfoliation process in 750m wall. ('Alone on the Wall' video still).

Steph Davis, also a famous free-solo expert, on sandstone. Note smoothness of the extensional fractures in the main face of the mountain wall. Stephdavis.co.

Fig. 14 Examples of sheeting joints on mountain faces of granite and sandstone

Relentless exfoliation due to temperature cycling, ice wedging and even the effect of relentless high winds. Cerro Torre, Fitz Roy peaks, Patagonia, Chile. (See detail on right).

Extensional strain, then ice-wedging and block-fall wedging emphasizes the impermanence of mountains and the top of Cerro Torre in particular. Patagonia, Chile.

An illustration of the role of variable geology on the 'longevity' of mountains. Note the slope debris from the mountain-side formed of jointed layers of volcanic rocks. Cerro Torre is the highest peak on the left. Patagonia, Chile.

Hans Florine, known as 'Hollywood Hans' to his friends, is shown with a time-lapse photograph in his King Swing traverse to a new crack system, on his 100th climb of The Nose, on El Capitan. The loose flake ('Boot Flake') presumably relies on high φ and low σ_n.

Fig. 15 Several examples of the widespread degradation of steep mountain sides, at different scales. The 'flake' at the side of the Patagonia peak is probably as long as 200 m, and presumably started as a minor extension process, followed by the continuous effects of temperature cycling, water pressure cycling, ice-wedging, and successively 'more successful' block-fall wedging of the inner-surface of the now huge crack. Bottom right is an unusual time-lapse photograph from the book by Florian and Moye (2016), and shows one of the wider (body-wide) cracks which exists behind the loosened and partly fallen so-called 'Boot Flake' on the famous 'Nose' route up the 1000 m high El Capitan face in Yosemite. There is another even larger 'flake' down to the right side called the 'Texas Flake' signifying the relentless degradation. Rock climbers are clearly oblivious to c, φ and σ_t/ν, and even bivouac on top of the larger, loose 'flakes' and 'towers'

some months of each year. In the Alps, specifically the Matterhorn, the gradual degradation of the highest rock which is in almost permafrost conditions, has been convincingly described by Weber et al. (2016).

Rock climbers actually depend on the process of geomorphological degradation (a) for the steepness of specific mountain walls in climbing mecca like Yosemite, Patagonia, Karakoram, etc., (b) for their best holds, i.e. for the most continuous near-vertical crack systems. The extension

strain origin of the latter represents a huge contribution to the existence of commercial rock-climbing gear, both for hobby and sports climbers, because devices for wedging into cracks exist in their thousands, and are sold in their millions. They are, for most climbers, a necessity for safer climbing, and represent a welcome substitute for first and second finger joints, fists, feet and whole bodies when behind loosened ('post-peak') flakes. Both the smooth, often continuous faces, and the long vertical cracks are the product, in effect, of vertical gravity-induced local 'tectonics'. They depend first on g, then tectonics, then H, γ, and ν, causing exceedance of critical extensional strain ε_c, and finally the insufficient tensile strength σ_t. The latter is inexorably reduced over time by diurnal and seasonal temperature fluctuation, with rain and ice in turn, causing water pressures and ice-wedging.

It is probably a 'sad reality', though not exactly a problem for this or the next many generations (of rock climbers) that the most impressive rock walls tend to be impressive because of their over-steepened state. This is because the proposed $\sigma_t/\gamma\nu$ mechanism of extension failure has the effect of maintaining the steepness, or even steepening and degrading existing mountain faces. An important initial steepening process may be the formation of cirques by active glaciers. The extension/slabbing mechanism clearly has assisted the rate of glacial steepening in such locations.

8 Mountain Heights: Why an Apparent 8–9 km Limit

Increasing the scale dramatically from the previously described 1-km high near-vertical mountain walls, one can tentatively suggest that the world's highest mountains (14 peaks of 8000 to almost 9000 m height) are also not 'limited' by the uniaxial compression strength of rock as sometimes proposed. Instead they need to be related to the limited shear strength as described by critical state, non-linear rock mechanics. (Barton 1976, 2013). Compression strength, if incorrectly applied, would anyway need to be the confined compression strength (σ_1 in Fig. 16), since great depth is obviously involved where stress and strength are (almost) in equilibrium. The possible range of perhaps 600–900 MPa confined compressive strength for strong igneous or metamorphic rocks at 10 km depth would support mountains of 20–30 km height, with the brittle–ductile transition long passed. The empirical evidence of millions of years is violated if trying to use the (confined) compression strength of the rock, and rock mechanics principles are violated by those suggesting use of the 200–300 MPa typical of uniaxial compressive strength.

Due to the non-linear behaviour of rock when shear stress is experienced, the upper bound limiting shear strength is

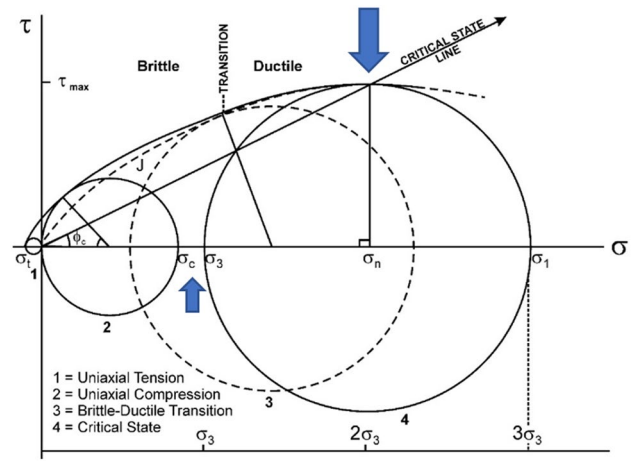

Fig. 16 Critical state diagram from Barton (1976). Singh et a. (2011) showed that the critical confining pressure (σ_3 on the left side of Mohr circle #4) was indistinguishable from the uniaxial compression strength σ_c (upward-pointing blue arrow). The downward-pointing blue arrow is our suggestion for the upper bound shear strength beneath high mountain ranges, but the maximum possible effective normal stress will be lower than shown due to the unknown but high pore pressure. This might have the practical effect of avoiding ductile behaviour

likely to be given by the top (horizontal) part of a relevant (intact) rock's shear strength envelope. (See largest vertical arrow in Fig. 16). In fact, and confusingly for those of us who are criticizing the use of uniaxial compression strength, the critical confining pressure (σ_3) needed to reach this upper bound shear strength, and the shear strength limit itself, have in fact the same numerical magnitude as the uniaxial compressive strength, such as 150, 200 or 250 MPa. From the geometry shown in Fig. 16, the upper bound shear strength would be numerically similar to uniaxial strength (in MPa) if a total normal stress as high as twice this value was generated at the 'base of the mountain'. The location of this equilibrium depth is uncertain due to isostatic uplift supporting the mountain chain. A photograph of Everest is shown in Fig. 17.

There are two further problems. First, there will be a high but unknown pore/joint water pressure at a nominal 10 km depth which might be as much as 50 MPa, but seems unlikely to be much higher due to laterally directed potential drainage from the steepest mountain flanks into the surrounding valleys. The magnitude of pore or joint water pressure is likely to be seasonal since frozen conditions can cut off supplies from above, perhaps for most of a Himalayan year. Second, the rock, even at 8–10 km depth will tend to be sheared and fractured in view of the tectonic forces acting against the Himalayas, so cannot actually reach the upper bound shear strength of intact rock, except perhaps where there are limited 'intact bridges' (if of potential kilometer size). Since the effective normal stress acting across a

potential inclined shear failure surface will be numerically less than $2 \times \sigma_c$ the available shear strength will be numerically less than $1 \times \sigma_c$, perhaps close to the brittle–ductile transition. This could also be a logical result.

The fourteen mountains in the exclusive 8–9 km height class provide empirical evidence of total vertical stresses that might be as high as $(9000 \times 3)/100$ MPa = 270 MPa, assuming a composite density as high as 3.0. If there could be a pore/joint water pressure as high as 50 MPa, then tentative application of the law of effective stress brings us to a principal effective vertical stress of 220 MPa close to the lower part of a potential shear surface. However, we need to consider the shear stress generated by this effective vertical stress of 220 MPa. On a plane inclined at 45° this could be as low as 150 MPa, considering round figures. In case of an elevated major horizontal stress (i.e. $K_0 > 1$), equilibrium would be improved, and a higher mountain could be supported before reaching a shear strength limit (Fig. 16).

The range of possible lower bound shear strengths beneath a mountain belt subject to tectonic stress as a result of plate boundary collisions is more or less certain to be higher than the shear strength associated with faults at near-residual strength, because such 'low shear strength' would deny the possibility of mountain building at such an adverse location. The final unknown is the form of shear failure surface(s) at depth beneath the mountain's highest peaks. What is the likely dip, and maybe curvature, of the height-limiting failure surface or surfaces? Are these surfaces, if they exist, a potential source of earthquakes?

9 Conclusions

1. Poisson's ratio and anisotropic stresses, causing extension strain and fracturing in tension, even with all principle stresses in compression, can explain the limited maximum heights of cliffs and steep mountain walls, and the origin of planar sheeting joints. Maximum heights ranging from 20 m in tuff, 100 m in chalk, 650 m in sandstone, to 1300 m in granite can be sensibly quantified by considering failure caused by extensional strain in each case.
2. There are parallels in the world of deep tunnels in hard rock. The widely quoted critical tangential stress of $0.4 \pm 0.1 \times \sigma_c$ that may signify fracture initiation in deep hard rock tunnelling can be replaced by the ratio σ_t/ν, i.e. initial tensile failure which is mobilized by Poisson's ratio causing extensional strain. These two ratios are, surprisingly and simply, arithmetically equivalent due to typical ratios of σ_c/σ_t (approx. 10) and Poisson's ratio (approx. 0.25).
3. It has been argued by others that a viable mechanism to explain the exfoliation slabbing, and 'flakes' (as referred in rock climbing) caused by sheeting joints, is surface curvature and the generation of tensile stresses. Since a huge proportion of slabs and flakes are nevertheless planar, sometimes over very large areas measuring 100's of meters in both directions, and since cracks may sometimes continue upwards for hundreds of meters (Fig. 18) another mechanism of origin for such (vertical) sheeting

Fig. 17 Mount Everest at 8848 m. (Photograph extracted from a larger Wikipedia photo). It is proposed that Mt. Everest's maximum height is shear strength limited, and ultimately limited by the critical state shear strength limit, as shown in Fig. 16. In fact differently inclined curved 'failure-planes' are apparent in this photograph, in front of the peak of Everest. Is it possible that these are the outer limits of curved failure surfaces through the next five kilometers of more obviously confined conditions? The curved non-parallel surfaces are unlikely to be related to bedding

Fig. 18 Free-solo climber Alex Honnold on El Capitan. Extension fractures are the assumed origin of these major, planar discontinuities

joints is needed, other than curvature. As in deep tunnels, the origin is likely to be extension fracturing, even with all three principal stresses compressive. Poisson's ratio is the frequent culprit, causing a critical tensile strain to be exceeded. Down a steep mountain face we can crudely equate the ratio σ_t/ν with an approximate principal stress, generated by height and density, and of course gravity.

4. As a result, the critical height of a vertical cliff can be roughly expressed as follows: $H_c = \sigma_t/\gamma\nu$ where γ is the rock density in appropriate units. This simple equation can be used to explain the world-wide limit of 1200–1300 m as the approximate range of the highest near-vertical mountain walls. The same equation can be used to predict failure of 10–20 m high cliffs in the very weak Cappadocia tuffs, where tensile strength may be < 0.1 MPa, compared to 5–10 MPa in the world's highest near-vertical mountain walls which are typically in granites.
5. Soil mechanics related formulæ starting with Coulomb, and involving the overcoming of cohesive strength, with lower bound and upper bound solutions depending on method of analysis (i.e. limit equilibrium or limit state), seriously over-estimate vertical cliff heights in rock by a factor of three to six times. This is because rock at large scale seldom fails like soil at much smaller scale. A uniaxial strength-based approximation suggested by Terzaghi (1962) has equal difficulty, and Terzaghi immediately proposed the need for the weakening effect of jointing to explain the gross over-estimation of his equation.
6. The world's highest mountains of 8000–9000 m are limited by maximum possible shear strength, not by compressive strength, because the confined compressive strength of competent mountain-forming rock is several times too high. Practical considerations of maximum vertical total stress, and transformation to maximum effective shear stress suggest that mountain height limits might be roughly consistent with the limits of the brittle–ductile transition of hard rock.
7. Shear strength and tensile strength (the latter ably assisted by Poisson's ratio) are inevitably the weakest links in, respectively, 'high-stress' structural geological processes on the one hand, and in the multitudes of 'low-stress' geomorphological processes that shape the details of rocky mountainous landscapes.

References

Addis MA, Barton N, Bandis C, Henry JP (1990) Laboratory studies on the stability of vertical and deviated boreholes. In: 65th Annual Technical Conference and Exhibition of the Society of Petroleum Engineers, New Orleans, September 23–26, 1990

Aydan Ö, Ulusay R (2003) Geotechnical and geoenvironmental characteristics of man-made underground structures in Cappadocia. Turk Eng Geol 69:245–272

Barton N (1976) The shear strength of rock and rock joints. Int J Rock Mech Min Sci Geomech Abstr 13:No. 9: 255–279

Barton N (1999) General report concerning some 20th Century lessons and 21st Century challenges in applied rock mechanics, safety and control of the environment. In: Proc. of 9th ISRM Congress, Paris, 3: 1659–1679, Balkema, Netherlands

Barton N (2013) Shear strength criteria for rock, rock joints, rockfill and rock masses: problems and some solutions. J of Rock Mech Geotech Engr Elsevier 5:249–261

Barton N, Grimstad E (2014) Q-system—an illustrated guide following forty years in tunnelling. 43 p. http://www.nickbarton.com

Barton N, Infanti N (2004) Unexpected stress problems in shallow basalts at the Ita hydroelectric power project in S.E. Brazil. Proc. ARMS 2004: 3rd Asian Rock Mechanics Symposium, Kyoto

Barton N, Shen B (2017) Risk of shear failure and extensional failure around over-stressed excavations in brittle rock. J Rock Mech Geotech Eng 9:210–225. https://doi.org/10.1016/j.jrmge.2016.11.004

Barton N, Warren C (1995) Rock mass classification of chalk marl in the UK Channel Tunnels. Channel Tunnel Engineering Geology Symp., Brighton

Bray JW (1967) A study of jointed and fractured rock. Part I. Fracture patterns and their failure characteristics. Felsmechanik 2–3:117–136

Byerlee JD (1967) Frictional characteristics of granite under high confining pressure. J Geophys Res 72:3639–3648

Byerlee JD (1968) Brittle-ductile transition in rocks. J Geophys Res 73:4741–4750

Davis S (2013) Learning to fly: an uncommon memoir of human flight, unexpected love, and one amazing dog. Simon & Schuster, New York

Drucker DC, Prager W (1952) Soil mechanics and plastic analysis or limit design. Q Appl Math 10:157–165

Florine H, Moye J (2016) On the Nose—A lifelong obsession with Yosemite's most iconic climb. Rowman & Littlefield, Lanham
Grimstad E, Barton N (1993) Updating of the Q-System for NMT. In: Proc. of Int. Symp. on Sprayed Concrete—Modern Use of Wet Mix Sprayed Concrete for Underground Support, Fagernes, 1993, Eds Kompen, Opsahl and Berg. Norwegian Concrete Association, Oslo, 46–66
Hall J, G Child (2002) Climbing Free. My life in the Vertical World. Harper Collins Publishers, New York
Honnold A, Roberts D (2016) Alone on the Wall. W.W. Norton & Company, New York
Martel SJ (2017) Progress in understanding sheeting joints over the past two centuries. J Struct Geol 94:68–86
Martin CD, Kaiser PK, McCreath DR (1998) Hoek–Brown parameters for predicting the depth of brittle failure around tunnels. Can Geotech J 36:136–151
Melosh HJ (2011) Planetary surface processes. Cambridge University Press, Cambridge
Mogi K (1966a) Some precise measurements of fracture strength of rocks under uniform compressive stress. Felsmechanik Ingenieurgeologie 4:41–55
Mogi K (1966b) Pressure dependence of rock strength and transition from brittle to ductile flow. Bull Earthq Res Inst Tokyo 44:215–232
Shen B, Barton N (2018) Rock fracturing mechanisms around underground excavations. J Geotech Eng Korea. (in press)
Shen B, Stephansson O, Rinne M (2013) Modelling rock fracturing processes: a fracture mechanics approach using FRACOD. Springer, Heidelberg
Shen B, Shi J, Barton N (2018) An approximate Non-Linear modified Mohr–Coulomb Shear strength criterion with critical state for intact rocks. J Rock Mech Geotech Eng. https://doi.org/10.1016/j.jrmge.2018.04.002
Singh M, Raj A, Singh B (2011) Modified Mohr–Coulomb criterion for non-linear triaxial and polyaxial strength of intact rocks. Int J Rock Mech Min Sci 48(4):546–555
Stacey TR (1981) A simple extension strain criterion for fracture of brittle rock. Int J Rock Mech Min Sci Geomech Abstr 18:469–474
Stacey TR, Xianbin Y, Armstrong R, Keyter GJ (2003) New slope stability considerations for deep open pit mines. Afr Inst Min Metall 103(6):373–389
Stock GM, Luco N, Collins BD, Harp EL, Reichenbach P, Frankel KL (2012) Quantitative rock-fall hazard and risk assessment for Yosemite Valley. Yosemite National Park, California
Terzaghi K (1962) Stability of steep slopes on hard unweathered rock. Geotechnique 12:251–263
Verruijt A (2001) Soil Mechanics. Delft University of Technology, The Netherlands
Weber S, Beutel J, Faillettaz J, Hasler A, Krautblatter M, Vieli A (2016) Quantifying irreversible movement in steep fractured bedrock permafrost at Matterhorn (CH). The Cryosphere Discussions Journal
Wolters G, Müller G (2008) Effect of cliff shape on internal stresses and rock slope stability. J Coastal Res 24(1), 43–50

Publisher's Note Springer Nature remains neutral with regard to jurisdictional claims in published maps and institutional affiliations.